Henderson, Thomas C.; Dekhil, Mohamed; Schenkat, Larry; Veigel, Larkin; Brüderlin, Beat:

Flat surface reconstruction using sonar

URN: urn:nbn:de:gbv:ilm1-2014210346

Published OpenAccess: November 2014

Original published in:

International journal of robotics research : IJRR. - Thousand Oaks, Calif : Sage Science Press (ISSN 1741-3176). - 17 (1998) 5, S. 504-511.

DOI: 10.1177/027836499801700503

URL: http://dx.doi.org/10.1177/027836499801700503

[Visited: 2014-10-14]

Flat Surface Reconstruction Using Sonar

Thomas C. Henderson, Mohamed Dekhil, Larry Schenkat, Larkin Veigel and Beat Brüderlin

The International Journal of Robotics Research 1998 17: 504
DOI: 10.1177/027836499801700503

Flat Surface Reconstruction Using Sonar

Thomas C. Henderson
Mohamed Dekhil
Larry Schenkat
Larkin Veigel
University of Utah
Salt Lake City, UT 84112, USA

Beat Brüderlin
Technical University of Ilmenau
D-98693 Ilmenau, Germany

Abstract

A technique is given for the recovery of planar surfaces using two spread-beam sonar readings. If a single planar surface gives rise to the two readings, the method recovers the surface quite accurately. Moreover, the technique provides information on the specular nature of the surface. Simulation and experiment demonstrate the effectiveness of the technique and recommend its use in practice.

1. Introduction

Sonar sensors in common use today (e.g., the Polaroid sensor) produce with reasonable accuracy the range to the nearest surface, but the direction to that surface is not explicitly determined; rather, the surface is known to lie within a certain spread of angle centered about the line of direction of the sensor (e.g., 22.5° for the Polaroid sensor; see Figure 1). Multiple sonar readings are required to disambiguate the location (pose) of the reflecting surface. Several researchers have investigated the use of sonar in mobile robotics (Bozma and Kuc 1991; Crowley 1985; Elfes 1987; Leonard and Durrant-Whyte 1991, 1992; Matthies and Elfes 1988), and others have directly addressed the problem of wall detection (Barshan and Kuc 1990; Borenstein and Koren 1995; Kleeman and Kuc 1995; Peremans, Audenaert, and Campenhout 1993), or have shown the minimum number and arrangement of sonar sensors to detect obstacles (Kuc 1990, 1991). However, no one has addressed the optimal pose recovery of planar surfaces in sonar data (see Henderson, Brüderlin, et al. 1996; Henderson, Dekhil, et al. 1996). In this paper, we address the simplest version of the k-wall/m-sonar (kWmS) problem:

> **Problem.** Given m sonar transmitter/receiver sensors situated on a circular ring placed in a k wall enclosure, what is the optimal sensing strategy to determine the pose of the k walls?

The International Journal of Robotics Research,
Vol. 17, No. 5, May 1998, pp. 504–511,

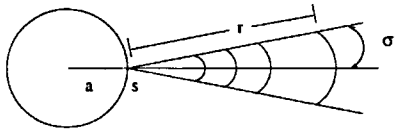

Fig. 1. Beam spread of sonar sensor.

The sonar sensor is assumed to have a nonzero beam spread (e.g., 22.5° degrees for a Polaroid sensor), and optimal is defined in terms of the recovery of the wall's pose with the minimum number of sensors used and moves made.

We start with the recovery of a single wall in the sensor's field of view. Given a single sonar sensor located on a circular ring at a distance a from the center of the ring, we show that two sonar readings, with one sensing position rotated with respect to the other (with certain conditions on the angle of rotation), suffice to recover the pose of a wall. This reduces to a plane geometry problem in which the wall is represented as a line in the plane, and its equation is determined.

This technique works for both specular and diffuse targets. The method can also be used to estimate the specular and diffuse nature of the target.

2. Pose Determination of a Wall

Assume that the environment consists of a single wall whose pose is to be determined (i.e., a line in the plane). There are three key insights:

1. A single sonar reading determines a set S of possible lines.
2. For the spread-beam sonar, S is qualitatively different than that from a narrow-beam sonar.

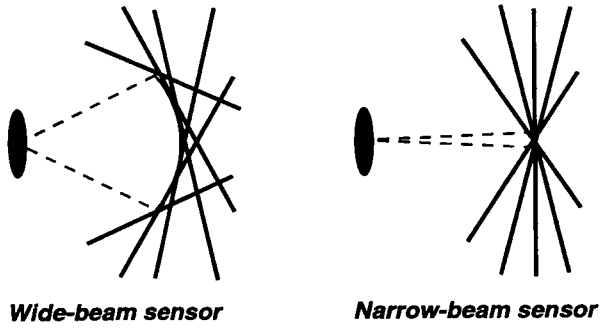

Fig. 2. Broad- and narrow-beam line set comparison.

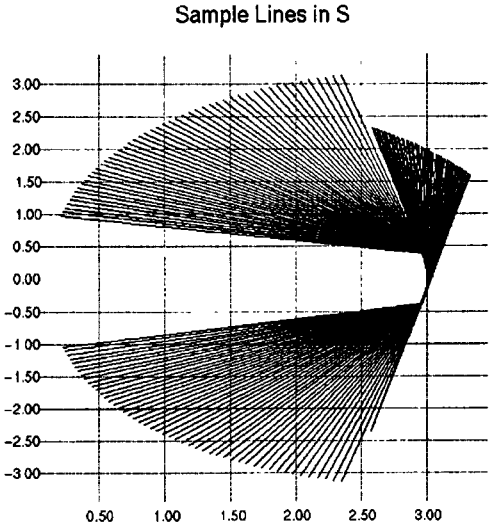

Fig. 3. Set of possible lines.

3. If correctly positioned, a second sonar reading can disambiguate which line in S gives rise to the two readings.

Figure 2 compares the broad-beam and narrow-beam line sets. For a narrow-beam sensor, only the orientation of the line is unknown, whereas for a broad-beam sensor, there are many possible positions and orientations of the line. Under certain conditions, there is a one-to-one relation between the second sonar reading and the lines in S. Figure 3 shows a sample set of lines for $a = 1$ and $r = 2$, whereas Figure 4 shows the sonar distance from a second sonar (rotated $-\pi/6$ from the first) to each of these lines; as can be seen, the plot of distance decreases monotonically, and this makes it possible to use the second sonar range to ascertain the line that gives rise to the two readings.

Suppose we are given a single sonar located at s on a circular platform of radius a as shown in Figure 1, and that it indicates a return at range r. The sensor is assumed to have a beam spread 2σ, and to reflect back a signal incident to a surface at any angle (the fact that there is in practice a minimum incident angle that gives a reflection will be accounted for later). Furthermore, assume that there is only one wall in the

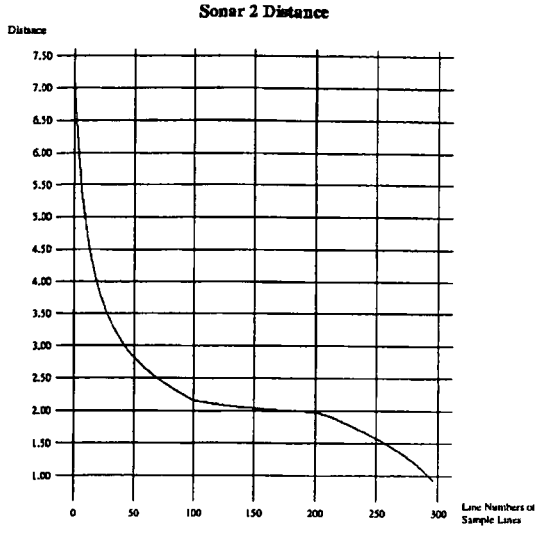

Fig. 4. Distance from second sonar to possible lines.

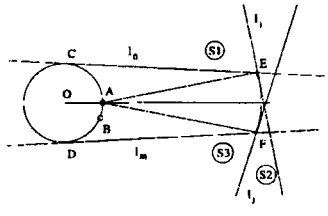

Fig. 5. Qualitative line sets.

vicinity of the sonar and it reflects a signal (i.e., it intersects the sonar wedge), and the wall may be a diffuse reflector.

Figure 5 shows the three qualitatively different sets of possible lines that could have produced a range reading of r. The qualitative line sets are as follows:

1. $S1$: The set of lines found by rotating (clockwise) l_0 about E into l_i.
2. $S2$: The set of lines found by sliding the tangent line along the circular arc EF from l_i to l_j.
3. $S3$: The set of lines found by rotating (clockwise) l_j about F into l_m.

We will show that the line that caused the range return value of r can be disambiguated by taking one more sonar reading after rotating the sonar sensor about the origin by an amount less than $\angle AEC$ (call this angle α) to the new position B. The sonar range distances from B to the lines in sets $S1$, $S2$, and $S3$ are monotonically decreasing, which permits a simple determination of the line that produced r (in fact, the discontinuities between the range to lines in $S1$ and lines in $S2$ can be seen at line 100 in Figure 4 and at line 200 for lines in $S2$ and $S3$).

Consider a clockwise rotation of angle θ of the sonar located at A rotated about O from A to B, where $0 < \theta < \alpha$

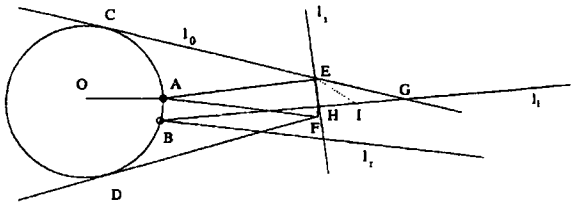

Fig. 6. $S1$ distances.

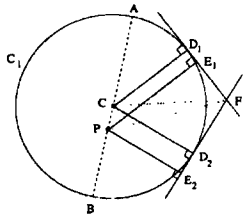

Fig. 7. Distance from P to the tangent lines ($S2$ lines).

(see Figure 6). Any ray in the second sonar scan to the right of l_l will intersect all lines in $S1$ at a greater distance than l_l will. In addition, the distance along l_l monotonically decreases to a line l as it starts at line l_0 and is rotated about E to line l_i. To see this, drop a perpendicular from E to segment $\overline{HG}$ of height $h = d \times \sin(\beta)$ (where $d = |\overline{EH}|$ and β is $\angle EHG$). It is clear that as segment $\overline{EG}$ rotates clockwise around E, segment $\overline{HI}$ goes monotonically to length zero, where point I is the intersection of lines l_i and l. (Note that the perpendicular to l_l through E is past l_i.) This follows from the fact that if $b = |\overline{HI}|$, the area of triangle $\triangle EHI$ monotonically decreases, so that $\frac{1}{2}bh$ decreases too, which implies that b does since h is constant.

We now show under what conditions the second sonar distance function is invertible. Consider the circle C_1 shown in Figure 7, with the point C being the location of the first sonar reading. Given a point P in the circle not at the center C, then the shortest distance from P to a tangent line to C_1 achieves a maximum at A, and a minimum to a tangent of the circle at B. This distance monotonically decreases for the tangent lines at points on C_1 as they range from A to B.

We will prove that the distance from the second sonar to the tangent lines along the arc AB decreases monotonically. Suppose not; then there exist two points D_1 and D_2 on the circle between A and B such that P is equidistant from the tangent lines to circle C_1 at D_1 and D_2 (i.e., $|PE_1| = |PE_2|$, where E_1 and E_2 are the points of intersection of the perpendiculars to the tangent lines at D_1 and D_2, respectively). Consider the two triangles PE_1F and PE_2F. We have

$$\overline{PF}^2 = \overline{PE_1}^2 + \overline{E_1F}^2 = \overline{PE_2}^2 + \overline{E_2F}^2. \quad (1)$$

From the assumption that $|\overline{PE_1}| = |\overline{PE_2}|$ and eq. (1), we have

$$|\overline{E_1F}| = |\overline{E_2F}|. \quad (2)$$

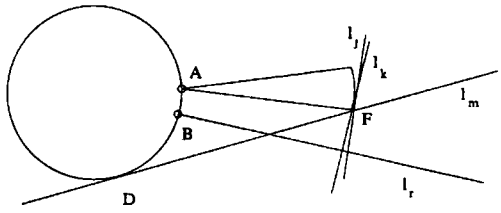

Fig. 8. $S3$ distances.

From the two triangles CD_1F and CD_2F, since $|\overline{CD_1}|$ and $|\overline{CD_2}|$ are equal (both equal to the radius of the circle C_1), and since $\overline{CF}$ is a common side in both triangles,

$$|\overline{D_1F}| = |\overline{D_2F}|. \quad (3)$$

Also, from Figure 7, we can see that

$$|\overline{E_1F}| = |\overline{D_1F}| - |\overline{D_1E_1}| \quad (4)$$

and

$$|\overline{E_2F}| = |\overline{D_2F}| + |\overline{E_2D_2}|. \quad (5)$$

Combining eqs. (2), (3), (4), and (5), we get

$$|\overline{D_1E_1}| + |\overline{E_2D_2}| = 0, \quad (6)$$

which means that $|\overline{D_1E_1}| = 0$ and $|\overline{D_2E_2}| = 0$, and so the two points E_1 and E_2 coincide with the two points D_1 and D_2, respectively. And since $\overline{PE_1}$ and $\overline{PE_2}$ are perpendiculars to the tangent lines of circle C_1, P must coincide with the center of the circle C, which contradicts the condition that P should be a point not at the center of the circle C_1.

For the final set of lines $S3$, we consider two subsets (Figure 8). Let l_k be the line between l_j and l_m which is perpendicular to l_r. Then, for all lines between l_k and l_m, as l_k is rotated around F to l_m, the shortest distance from B to the line is along a line clockwise from l_r; therefore, for those lines, the shortest distance in the sonar wedge from B is along line l_r and monotonically decreases.

Finally, for the lines from l_j to l_k, we claim that the shortest distance from B decreases monotonically. Suppose not; then there exist two points J_1 and J_2 such that the distance d to B is the same. Since for this set of lines the shortest distance is on the perpendicular to B, there exist two tangent lines to the circle centered at B of radius d such that both lines go through F and are on the same side of the circle: $\otimes$.

Thus, we have shown that given the set of lines that could cause a sonar return of r from a single wall, a second sonar return from a rotated location is sufficient to disambiguate the pose of the wall. However, the proof has imposed two conditions on the rotated position:

- The angle between the first and second sonar locations cannot exceed α, the angle between the lines l_0 and $\overleftrightarrow{AE}$ (Figure 6).
- The line $\overleftrightarrow{BA}$ (Figure 7) should not cut the arc EF (Figure 6).

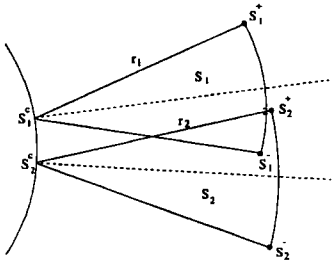

Fig. 9. Notation used in the algorithm.

As long as the sonar sensor is rotated a nonzero amount about the center of the nonzero radius sonar ring, but less than the angle made by a tangent to the robot that goes through the sector corners, the pose of the wall can be found, and the proof applies. C and P play the roles of the first and second sonar locations, respectively.

3. An Implementation

Given two sonar readings r_1 and r_2, we can determine the pose of the wall, assuming that the wall is flat and in the field of view of both sensors. First, let us define some points as shown in Figure 9. Two sensors are located on a circular arc at locations S_1^c and S_2^c, with fields of view represented by the two sectors S_1 and S_2, respectively. The corners of each sector are defined by the points S_i^+ and S_i^- as shown in Figure 9.

A simple solution is to use bisection search on the set of lines to find the line at (sonar) distance r_2 from S_2^c. Another approach is to separate the line set into qualitatively distinct categories. There are five different cases for the orientation of the wall with respect to the two sensors. These cases are shown in Figures 10–14 and can be summarized as follows:

CASE 1: The wall is tangent to neither sector arc and goes through S_1^+ and S_2^+.

CASE 2: The wall is tangent to S_1 but not to S_2 and goes through S_2^+.

CASE 3: The wall is tangent to arcs of both S_1 and S_2.

CASE 4: The wall is tangent to S_2 but not to S_1 and goes through S_1^-.

CASE 5: The wall is tangent to neither sector arc and goes through S_1^- and S_2^-.

For each of these cases, by fixing r_1, the value of r_2 can determine which region the wall is in. The following algorithm can be used to determine the wall pose given the two sensor readings r_1 and r_2.

- If $r_1 \leq r_2$,

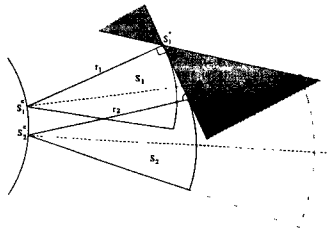

Fig. 10. First region.

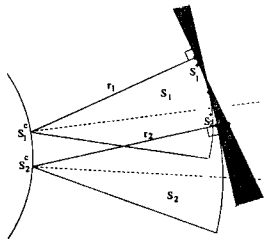

Fig. 11. Second region.

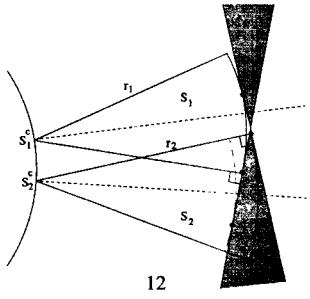

Fig. 12. Third region.

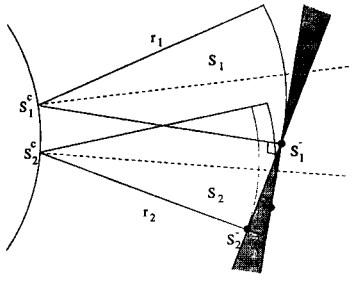

Fig. 13. Fourth region.

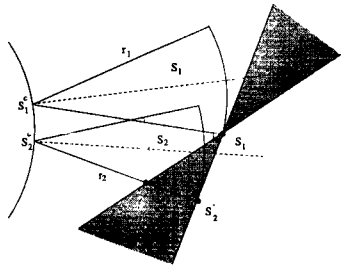

Fig. 14. Fifth region.

1. draw a tangent line from point S_1^+ to the arc of sector S_1 (see Figure 10);
2. if the distance from point S_2^c to that tangent along the line $\overline{S_2^c S_2^+}$ is less than or equal to r_2, the wall is in the first region and is represented by the line segment connecting S_1^+ and S_2^+;
3. or else, draw a tangent to the arc of sector S_2 from point S_2^+, as shown in Figure 11;
4. if the distance from the point S_1^c to that tangent is greater than or equal to r_1, the wall is in the second region, and the tangent to sector S_1 that goes through S_2^+ represents the wall;
5. or else, the wall is in the third region (Figure 12) and is represented by the common tangent to the two arcs.

- Or else, if $r_1 > r_2$,

1. draw a tangent line from point S_2^- to the arc of the sensor at S_2 (see Figure 14);
2. if the distance from point S_1^c to that tangent along the line $\overline{S_1^c S_1^-}$ is less than or equal to r_1, the wall is in the fifth region and is represented by the line segment connecting S_1^- and S_2^-;
3. or else, draw a tangent to the arc of sector S_1 from point S_1^-, as shown in Figure 13;
4. if the distance from the point S_2^c to that tangent is greater than or equal to r_2, the wall is in the fourth region, and the tangent to sector S_2 that goes through S_1^- represents the wall;
5. or else, the wall is in the third region (Figure 12) and is represented by the common tangent to the two arcs.

The only task that remains is to find the common tangent to two circles. Figure 15 shows the basic idea of finding the common tangent. We connect the two centers C and P and extend the line segment $\overline{CP}$ to F where the distance $|\overline{PF}|$ can be calculated from the equality

$$\frac{r_1}{r_2} = \frac{|\overline{FC}|}{|\overline{FP}|}, \tag{7}$$

where

$$|\overline{FC}| = |\overline{FP}| - |\overline{CP}|. \tag{8}$$

From point F, we draw a line that makes an angle of θ with the line $\overline{FP}$, where

$$\sin\theta = \frac{|r_2 - r_1|}{|\overline{CP}|}. \tag{9}$$

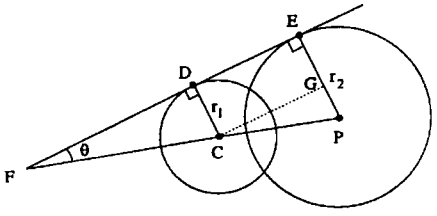

Fig. 15. Finding the common tangent of two circles.

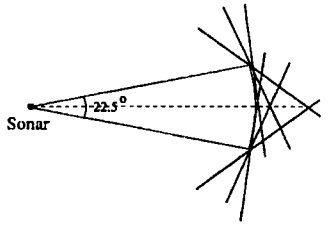

Fig. 16. Reference wall experiment.

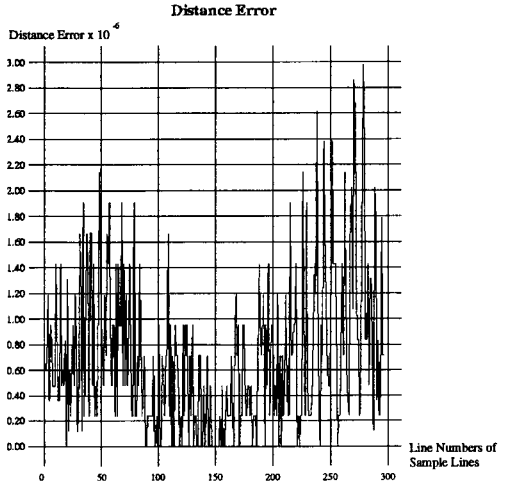

Fig. 17. Synthetic data: distance.

4. Experimental Results

In practice, sonar sensors located on a ring and with at most 18° difference in their directions can be used pairwise to recover hypotheses about walls present in the environment (this is because a sonar-wall incident angle of greater than 60° is necessary to get a return with the Polaroid sensor). We present here some experimental data taken with walls located in known positions with respect to the sonar ring and compare the calculated poses.

First, we consider the setup shown in Figure 16. A simulation of this setup results in the error curves shown in Figure 17 (distance) and Figure 18 (angle). This error is a result of numerical round-off error.

In the experiment, a wall (a large modular office partition

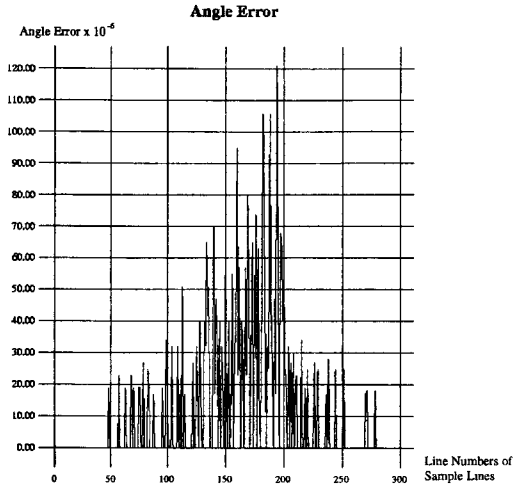

Fig. 18. Synthetic data: orientation.

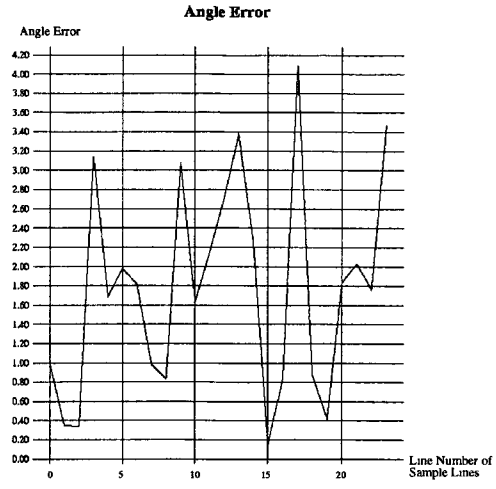

Fig. 20. Experimental data: orientation.

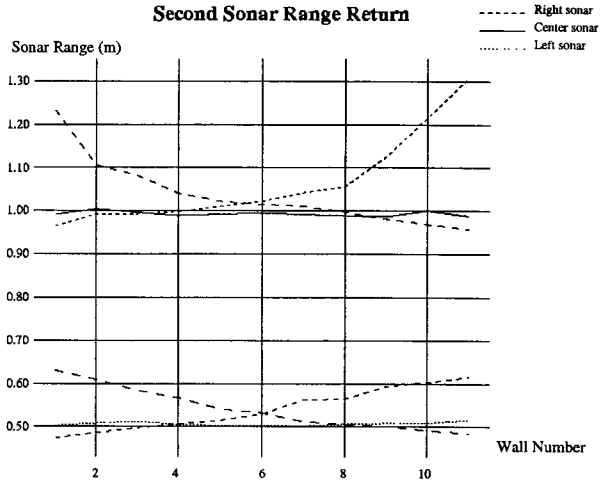

Fig. 19. Controlled line recovery data.

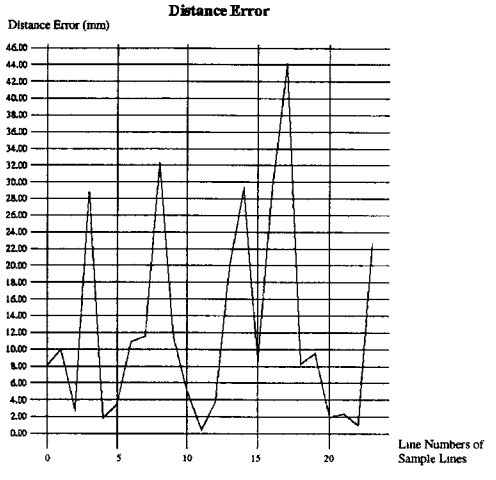

Fig. 21. Experimental data: distance.

wall) was placed at a fixed distance d but at various tangents to the circle of radius d centered at the sonar sensor S_1. A reading was then taken from the second sonar sensor S_2, and the pose was calculated. Figure 19 shows the range reading from a central sonar and two side sonars placed at 1 m and 0.5 m and clearly indicates the stability of the range of the central sonar and the monotonic nature of the two side sonars.

In the next experiment, the robot interacted with actual walls in an office. The pose of the walls was measured with respect to a frame in which the center of the sonar ring is in the origin and the location of the front sonar is the x-axis. Figure 20 shows the angle error between the computed wall orientation and the actual wall orientation. Figure 21 shows the distance error between the computed wall and the actual wall (where distance is the normal distance from the origin to the wall).

In addition, we compared our method with a more standard approximation used in the mobile robot community. A pose estimate can be made by assuming there is no beam spread on the sonar, so that two distinct points on the wall are given by the orientation and range of the two sonar readings. The line is then defined by these two points. A comparison of the error in this method and the error in our method is given in Figures 22 and 23.

5. Conclusions

This paper presents a sonar-sensing strategy in which sonar readings from specular or diffuse targets recover wall positions in the environment. This technique can be used to

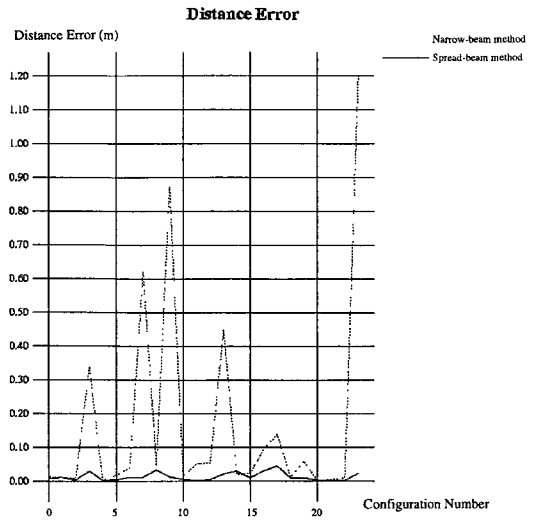

Fig. 22. Method comparison: distance.

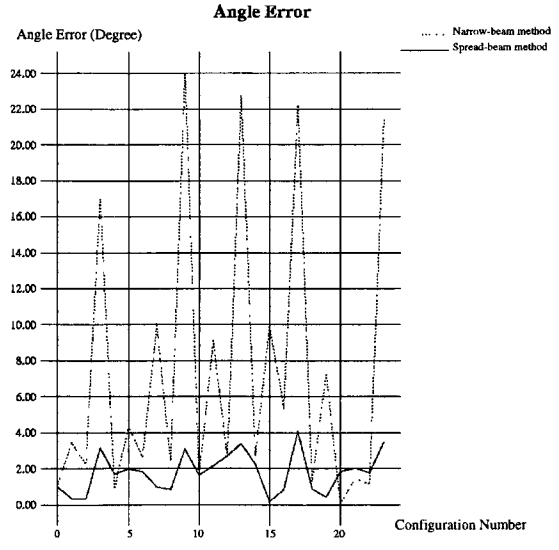

Fig. 23. Method comparison: orientation.

generate hypotheses about wall surface phenomena and develop strategies based on those hypotheses. The underlying geometrical arguments may also be relevant to other kinds of sensors with similar spread-beam physics.

We have presented what we believe to be an optimal solution to the 1W1S problem. We have demonstrated its effectiveness on synthetic data and on actual Polaroid sonar data. We have shown that the line estimates for two range sensor readings produced by this method are more accurate than line estimates from the two points obtained simply by using the sensor orientation and range in that direction (as suggested by Kuc 1990: "A sonar map is generated by placing a dot at the computer range along the transducer orientation").

The error in the actual data is due to both the error in the range readings and the numerical error involved in the computation. The minimum incident angle does not need to be accounted for, since the method produces only a flat surface hypothesis for two neighboring sonar sensors that both produce a range value (for more details, see Henderson, Brüderlin, et al. 1996).

Given that the smallest angle that provides a sonar return is about 60°, it is necessary to have at least 20 sonar sensors equally spaced and no more than 18° apart to be able to detect a wall within sonar range of a mobile platform (also see Kuc 1991). Our particular Labmate has a 24-sonar ring with sensors spaced 15° apart and was used for the experiments described here. The idea is that this method permits hypothesis testing on any possible wall. The hypotheses can then be refined by moving and taking more readings.

We are also studying the kWmS problem in more generality. We believe that the equations and specific constraints can be solved in the multiple wall, multiple sonar case as well. It may be possible to use the 1W1S solution with additional hypotheses (e.g., two walls at a given angle) to solve the more general problem.

Acknowledgments

We would like to thank Professor William Thompson for discussions about this technique. This work was supported in part by the Advanced Research Projects agency under Army Research Office grant DAAH04-93-G-0420 and by NSF grant CDA 9024721.

References

Barshan, B., and Kuc, R. 1990. Differentiating sonar reflections from corners and planes by employing an intelligent sensor. *IEEE Trans. Pattern Analysis and Machine Intelligence* 12(6):560–569.

Borenstein, J., and Koren, Y. 1995. Error eliminating rapid ultrasonic firing mobile robot obstacle avoidance. *IEEE J. Robotics and Automation* 11:132–138.

Bozma, O., and Kuc, R. 1991. Building a sonar map in a specular environment using a single mobile sensor. *IEEE Trans. Pattern Analysis and Machine Intelligence* 13(12):1260–1269.

Crowley, J. 1985. Navigation for an intelligent robot. *IEEE J. Robotics and Automation* RA-1(1):31–41.

Elfes, A. 1987. Sonar-based real-world modeling and navigation. *IEEE Trans. Robotics and Automation* RA-3(3):249–265.

Henderson, T. C., Brüderlin, B., Dekhil, M., Schenkat, L., and Veigel, L. 1996 (Minneapolis, MN, April). Sonar sensing strategies. *IEEE Int. Conf. Robotics and Automation*, pp. 341–346.

Henderson, T. C., Dekhil, M., Brüderlin, B., Schenkat, L., and Veigel, L. 1996 (Palm Springs, CA, February).

Flat surface reconstruction using minimal sonar readings. *DARPA Image Understanding Workshop*, pp. 995–1000.

Kleeman, L., and Kuc, R. 1995. Mobile robot scanner for target localization and classification. *Int. J. Robotics Research* 14(4):295–318.

Kuc, R. 1990. A spatial sampling criterion for sonar obstacle detection. *IEEE Trans. Pattern Analysis and Machine Intelligence* 12(7):686–690.

Kuc, R. 1991. A physically based navigation strategy for sonar guided vehicles. *Int. J. Robotics Research* 10(2):75–87.

Leonard, J. J., and Durrant-Whyte, H. F. 1991. Mobile robot localization by tracking geometric beacons. *IEEE J. Robotics and Automation* 7(3):376–382.

Leonard, J. J., and Durrant-Whyte, H. F. 1992. *Directed Sonar Sensing for Mobile Robot Navigation.* Boston: Kluwer Academic.

Matthies, L., and Elfes, A. 1988 (Philadelphia, April). Integration of sonar and stereo range data using a grid-based representation. *IEEE Int. Conf. Robotics and Automation*, pp. 727–733.

Peremans, H., Audenaert, K., and Campenhout, J. V. 1993. A high-resolution sensor based on tri-aural perception. *IEEE Trans. Robotics and Automation* 9(1):36–48.